ARCHIVES OF ELECTRICAL ENGINEERING VOL. 66(1), pp. 55-75 (2017)

DOI 10.1515/aee-2017-0005

A new algebraic LQR weight selection algorithm for tracking control of 2 DoF torsion system

VINODH KUMAR ELUMALAI[1], RAAJA GANAPATHY SUBRAMANIAN[2]

[1]*School of Electrical Engineering, VIT University*
Vellore, Tamilnadu, 632014, India
e-mail: vinothmepsg@gmail.com

[2]*Eindhoven University of Technology*
5612 AZ Eindhoven, the Netherlands
e-mail: raaja1393@gmail.com

(Received: 30.12.2015, revised: 19.07.2016)

Abstract: This paper proposes a novel linear quadratic regulator (LQR) weight selection algorithm by synthesizing the algebraic Riccati equation (ARE) with the Lagrange multiplier method for command following applications of a 2 degree of freedom (DoF) torsion system. The optimal performance of LQR greatly depends on the elements of weighting matrices $\boldsymbol{Q}$ and $\boldsymbol{R}$. However, normally these weighting matrices are chosen by a trial and error approach which is not only time consuming but cumbersome. Hence, to address this issue, blending the design criteria in time domain with the ARE, we put forward an algebraic weight selection algorithm, which makes the LQR design both simple and modular. Moreover, to estimate the velocity of a servo angle, a high gain observer (HGO) is designed and integrated with the LQR control scheme. The efficacy of the proposed control scheme is tested on a benchmark 2 DoF torsion system for a trajectory tracking application. Both the steady state and dynamic characteristics of the proposed controller are assessed. The experimental results accentuate that the proposed HGO based LQR scheme can guarantee the system to attain the design requirements with minimal vibrations and tracking errors.

Key words: ARE, high gain observer, LQR, $\boldsymbol{Q}$ and $\boldsymbol{R}$ matrices, 2 DoF torsion system, trajectory tacking

1. Introduction

Due to their inherent stability and robustness characteristics, Linear Quadratic Regulator, a cornerstone of Model Predictive Control and Linear Quadratic Guassian/Loop Transfer Re-

covery (LQG/LTR) Control, finds its applications in many of the engineering and scientific domains [1-2]. The LQR technique is a structured control technique, which can be easily extended to a multi variable system. Moreover, minimizing the quadratic cost function which integrates both states and inputs of the system via penalty matrices, LQR offers an optimal response between speed of response and amount of control input. In the last few decades, several results on LQR: hybrid LQR [3], fuzzy LQR [4], switched LQR [5], to name a few, have been reported in the literature. Moreover, LQR has been successfully applied for a large number of complex systems namely, a double inverted pendulum [6], fuel cell systems [6], and aircraft [7].

However, two major challenges of the LQR design have been the subject of investigation in the last five decades: the choice of $\boldsymbol{Q}$ and $\boldsymbol{R}$ weighting matrices, and the solution of ARE. Both the tasks are known to be highly dependent on the dynamic order of the system and certain operational condition. Since the optimal performance of LQR largely depends on weighting matrices, several results have been reported on optimal selection of $\boldsymbol{Q}$ and $\boldsymbol{R}$ matrices. Sunar and Rao [9], initializing the design variable as diagonal entries of $\boldsymbol{Q}$ and $\boldsymbol{R}$ matrices, proposed a methodology for selecting the state and input matrices of LQR applied to integrated structure design. To save the computational cost with minimal loss in accuracy, they used a substructure decomposition technique. Ohta et al. [10], as an alternate approach, investigated the inverse problem of the LQR controller for a single input system. As a simulation study on a roll autopilot system, they proved that the performance of LQR could be improved if negative diagonal state weights were used in the performance index. Ochi and Kani [11] put forward a new way of placing the LQR poles by solving the differential equations obtained from the Hamilton matrix. Even though this method guarantees that the poles can be located exactly at the desired positions, it does not assure the positive definiteness of the weighting matrix. Moreover, the method does not consider the eigen vector assignment problem and is computationally expensive. Based on the asymptotic modal properties of multivariable LQ regulators, Hiroe et al. [12] proposed a zero addition decoupling (ZED) method, to select the weights of the LQ regulator. The validity of the ZED method was demonstrated on a decoupleing control of an industrial turbine. Choi and Seo [13] presented a new LQR design technique which has the capability to assign not only the eigen values to the desired location but eigen vectors in the least square sense. Moreover, this method can also guarantee the frequency domain characteristics of conventional LQR. Ang et al. [14], using modal control analysis to assess the effect of energy weights on damping ratios, put forward a finite element LQR control technique and applied to vibration control of piezoelectric composite plates. As an alternate approach, several authors have also assessed the efficacy of evolutionary computation techniques like GA and PSO to solve the LQR optimization problem. For instance, Robanti et al. [15] investigated the efficacy of GA to solve the weight optimization problem of LQR on a multi-machine power system. Comparing the performance of GA optimized LQR with those of Bryson's method and a trial and error based method, they reported that the weights optimized via GA yield the best response of all three methods. However, high computational cost and large number of parameter tuning make GA less competitive than particle swarm optimization (PSO). Panda and Pathy [16], comparing the performance of both GA and

PSO based controller designs for a flexible AC transmission system, reported that the PSO based controller yields better performance than that of GA. Similarly, Tasi et al. [17] employed PSO to optimize the gains of a state feedback controller and proved that the tracking performance of PSO optimized LQR is better than that of the linear matrix inequality (LMI) based LQR for automatic fighter tracking problems. Kumar and Jerome [18], utilizing adaptive PSO(APSO) to solve the LQR weight optimization problem and validating the performance of APSO optimized LQR on a benchmark inverted pendulum, reported that the performance of APSO based LQR is better than those of PSO and GA based LQRs.

Nevertheless, high dependency on the parameters of the optimization problem and high computation time limit the use of evolutionary computation technique to solve many of the real world optimization problem. Hence, in this paper, we make an attempt to solve the weight selection problem of LQR by exploring the fundamental relation between the ARE and the Lagrange optimization technique. Computing the solution of ARE, the transformation matrix, as a function of design requirement in time domain and state model, the proposed algebraic approach yields simple mathematical relations for $\boldsymbol{Q}$ and $\boldsymbol{R}$ matrices. The proposed algebraic weight selection algorithm is tested on a benchmark Quanser 2 DoF torsion system for reference following applications. 2 DoF torsion system, which consists of torsional load attached to the shaft of the DC motor via flexible coupling, emulates the dynamics of high gear ratio harmonic drives and light weight transmission shafts. The control objective is to position the torsion module to the desired angle by manipulating the control input given to the DC servo. The system also consists of, along with the optical encoders attached to the shaft and torsion module measure the angular positions, an HGO to estimate the angular velocities. The weights of the LQR are optimized using the proposed algebraic approach and the dynamic and steady state characteristics of the LQR controller framework to follow the reference input is assessed for two test cases namely: sine and square inputs.

The remainder of the paper is structured as follows: Section 2 gives the problem definition and Section 3 describes the algebraic approach for choosing the elements of $\boldsymbol{Q}$ and $\boldsymbol{R}$ matrices based on ARE. Section 4 presents the modeling of the 2-DoF torsion system and the HGO based LQR design control scheme. Section 5 explains the experimental results of the 2 DoF torsion system for tracking applications, and the paper ends with the concluding remarks in Section 6.

2. Problem definition

Consider a linear time invariant (LTI) multivariable system:

$$\dot{\mathbf{X}} = \mathbf{A}\boldsymbol{X}(t) + \mathbf{B}\mathbf{u}(t), \quad t \geq 0, \quad \boldsymbol{X}(0) = \boldsymbol{X}_0, \tag{1}$$

$$\boldsymbol{Y} = \boldsymbol{C}\boldsymbol{X}(t) + \boldsymbol{D}\boldsymbol{u}(t), \quad t \geq 0, \tag{2}$$

where $\boldsymbol{A} \in R^{n\times n}$, $\boldsymbol{B} \in R^{n\times m}$, $\boldsymbol{C} \in R^{p\times n}$, $\boldsymbol{D} \in R^{p\times m}$ are system matrix, input matrix, output matrix and feed-forward matrix, respectively. $\boldsymbol{X}$ is the state vector, $\boldsymbol{u}$ is the control input vector, and $\boldsymbol{Y}$ is the output vector. The objective of the conventional LQR design is to take the states to the desired trajectory by minimizing the following cost function.

$$J(\boldsymbol{u}) = \int_0^{\infty} \left[\boldsymbol{X}^T(t)\boldsymbol{Q}\boldsymbol{X}(t) + \boldsymbol{u}^T(t)\boldsymbol{R}\boldsymbol{u}(t) \right] \mathrm{d}t \,, \tag{3}$$

where $\boldsymbol{Q}$ and $\boldsymbol{R}$ are state and input weighting matrices. The compositions of $\boldsymbol{Q}$ and $\boldsymbol{R}$ elements have large influence on system performance. If the weighting matrices are selected as diagonal matrices, the quadratic performance index is simply a weighted integral of the states and inputs [19]. These weighting matrices are considered as the tuning parameters of LQR by observing $\boldsymbol{Q}$ as state error penalty and $\boldsymbol{R}$ as penalty on control input. The elements of $\boldsymbol{Q}$ and $\boldsymbol{R}$ matrices depend on the number of state and input variables respectively. For the LQR to yield stable response, $\boldsymbol{Q}$ should be a positive semi definite matrix and $\boldsymbol{R}$ should be a positive definite matrix. The solution of following ARE, transformation matrix $\boldsymbol{P}$, can be used to obtain the state feedback gain of LQR.

$$\boldsymbol{A}^T\boldsymbol{P} + \boldsymbol{P}\boldsymbol{A} + \boldsymbol{Q} - \boldsymbol{P}\boldsymbol{B}\boldsymbol{R}^{-1}\boldsymbol{B}^T\boldsymbol{P} = 0 \,. \tag{4}$$

LQR computes the optimal control input given in (5).

$$\boldsymbol{u} = -\boldsymbol{K}\boldsymbol{X} \,, \tag{5}$$

where $\boldsymbol{K}$ is the state feedback gain matrix determined using the following Lagrange multiplier optimization technique.

$$\boldsymbol{K} = \boldsymbol{R}^{-1}\boldsymbol{B}^T\boldsymbol{P} \,. \tag{6}$$

Since the choice of $\boldsymbol{Q}$ and $\boldsymbol{R}$ weighting matrices affect convergence of a quadratic function, it is important to select these matrices by ensuring that both the state and input constraints are met in addition to the stability criteria [20]. However, normally, a trial and error method is used to choose the values of $\boldsymbol{Q}$ and $\boldsymbol{R}$ matrices, which is laborious and time consuming. Hence, to address this weight selection problem in the following section, we formulate an algebraic approach to arrive at simple mathematical relations for these weighting matrices.

3. Algebraic approach for *Q* and *R* matrices selection

Consider an LTI system represented in controllable canonical form as given below.

$$\dot{\mathbf{X}} = \begin{bmatrix} 0 & 1 & 0 & 0 & 0 & 0 \\ 0 & 0 & 1 & 0 & 0 & 0 \\ 0 & 0 & 0 & 1 & 0 & 0 \\ 0 & 0 & 0 & 0 & 1 & 0 \\ 0 & 0 & 0 & 0 & 0 & 1 \\ A_{61} & A_{62} & A_{63} & A_{64} & A_{65} & A_{66} \end{bmatrix} \begin{bmatrix} x_1 \\ x_2 \\ x_3 \\ x_4 \\ x_5 \\ x_6 \end{bmatrix} + \begin{bmatrix} 0 \\ 0 \\ 0 \\ 0 \\ 0 \\ B_{61} \end{bmatrix} \mathbf{u} . \tag{7}$$

We formulate the methodology with the assumption that the system (A, B, C) is both controllable and observable. Selecting the penalty matrices $\boldsymbol{Q}$ and $\boldsymbol{R}$ as diagonal matrices reduces the cost function to a quadratic term and simplifies the optimization problem. Hence, the penalty matrices are assumed to be:

$$\boldsymbol{Q} = \begin{bmatrix} q_1 & 0 & 0 & 0 & 0 & 0 \\ 0 & q_2 & 0 & 0 & 0 & 0 \\ 0 & 0 & q_3 & 0 & 0 & 0 \\ 0 & 0 & 0 & q_4 & 0 & 0 \\ 0 & 0 & 0 & 0 & q_5 & 0 \\ 0 & 0 & 0 & 0 & 0 & q_6 \end{bmatrix}, \quad \boldsymbol{R} = [r] . \tag{8}$$

The solution of ARE, transformation matrix $\boldsymbol{P}$, is a symmetric matrix, which can be represented as:

$$\boldsymbol{P} = \begin{bmatrix} p_{11} & p_{12} & p_{13} & p_{14} & p_{15} & p_{16} \\ p_{12} & p_{22} & p_{23} & p_{24} & p_{25} & p_{26} \\ p_{13} & p_{23} & p_{33} & p_{34} & p_{35} & p_{36} \\ p_{14} & p_{24} & p_{34} & p_{44} & p_{45} & p_{46} \\ p_{15} & p_{25} & p_{35} & p_{45} & p_{55} & p_{56} \\ p_{16} & p_{26} & p_{36} & p_{46} & p_{56} & p_{66} \end{bmatrix} . \tag{9}$$

Substituting the weighting matrices and a transformation matrix in (6) yields

$$\boldsymbol{K} = \boldsymbol{R}^{-1}\boldsymbol{B}^T \quad \boldsymbol{P} = \frac{B_{61}}{r}\begin{bmatrix} p_{16} & p_{26} & p_{36} & p_{46} & p_{56} & p_{66} \end{bmatrix}. \tag{10}$$

The coefficients of $\boldsymbol{P}$ matrix, namely p_{16}, p_{26}, p_{36}, p_{46}, p_{56} and p_{66}, can be obtained using the ARE given in (11).

$$\left\{\begin{bmatrix} 2(p_{16}A_{61})+q_1 - \frac{B_{61}^2}{r}p_{16}^2 & A_{61}p_{26}+p_{11}+p_{16}A_{62}-\frac{B_{61}^2}{r}p_{26}p_{16} & A_{61}p_{36}+p_{12}+p_{16}A_{63}-\frac{B_{61}^2}{r}p_{36}p_{16} & A_{61}p_{46}+p_{13}+p_{16}A_{64}-\frac{B_{61}^2}{r}p_{46}p_{16} & A_{61}p_{56}+p_{14}+p_{16}A_{65}-\frac{B_{61}^2}{r}p_{56}p_{16} & A_{61}p_{66}+p_{15}+p_{16}A_{66}-\frac{B_{61}^2}{r}p_{66}p_{16} \\ A_{61}p_{26}+p_{11}+p_{16}A_{62}-\frac{B_{61}^2}{r}p_{26}p_{16} & 2(p_{26}A_{62}+p_{12})+q_2-\frac{B_{61}^2}{r}p_{26}^2 & A_{62}p_{36}+p_{13}+p_{26}A_{63}+p_{22}-\frac{B_{61}^2}{r}p_{36}p_{26} & A_{62}p_{46}+p_{14}+p_{26}A_{64}+p_{23}-\frac{B_{61}^2}{r}p_{46}p_{26} & A_{62}p_{56}+p_{15}+p_{26}A_{65}+p_{24}-\frac{B_{61}^2}{r}p_{56}p_{26} & A_{62}p_{66}+p_{16}+p_{26}A_{66}+p_{25}-\frac{B_{61}^2}{r}p_{66}p_{26} \\ A_{61}p_{36}+p_{12}+p_{16}A_{63}-\frac{B_{61}^2}{r}p_{36}p_{16} & A_{62}p_{36}+p_{13}+p_{26}A_{63}+p_{22}-\frac{B_{61}^2}{r}p_{36}p_{26} & 2(p_{36}A_{63}+p_{23})+q_3-\frac{B_{61}^2}{r}p_{36}^2 & A_{63}p_{46}+p_{24}+p_{36}A_{64}+p_{33}-\frac{B_{61}^2}{r}p_{46}p_{36} & A_{63}p_{56}+p_{25}+p_{36}A_{65}+p_{34}-\frac{B_{61}^2}{r}p_{56}p_{36} & A_{63}p_{66}+p_{26}+p_{36}A_{65}+p_{36}-\frac{B_{61}^2}{r}p_{66}p_{36} \\ A_{61}p_{46}+p_{13}+p_{16}A_{64}-\frac{B_{61}^2}{r}p_{46}p_{16} & A_{62}p_{46}+p_{14}+p_{26}A_{64}+p_{23}-\frac{B_{61}^2}{r}p_{46}p_{26} & A_{63}p_{46}+p_{24}+p_{36}A_{64}+p_{33}-\frac{B_{61}^2}{r}p_{46}p_{36} & 2(p_{46}A_{64}+p_{34})+q_4-\frac{B_{61}^2}{r}p_{46}^2 & A_{64}p_{56}+p_{35}+p_{46}A_{65}+p_{44}-\frac{B_{61}^2}{r}p_{56}p_{46} & A_{64}p_{66}+p_{36}+p_{46}A_{66}+p_{45}-\frac{B_{61}^2}{r}p_{66}p_{46} \\ A_{61}p_{56}+p_{14}+p_{16}A_{65}-\frac{B_{61}^2}{r}p_{56}p_{16} & A_{62}p_{56}+p_{15}+p_{26}A_{65}+p_{24}-\frac{B_{61}^2}{r}p_{56}p_{26} & A_{63}p_{56}+p_{25}+p_{36}A_{65}+p_{34}-\frac{B_{61}^2}{r}p_{56}p_{36} & A_{64}p_{56}+p_{35}+p_{46}A_{65}+p_{44}-\frac{B_{61}^2}{r}p_{56}p_{46} & 2(p_{56}A_{65}+p_{45})+q_5-\frac{B_{61}^2}{r}p_{56}^2 & A_{65}p_{66}+p_{46}+p_{56}A_{66}+p_{55}-\frac{B_{61}^2}{r}p_{66}p_{56} \\ A_{61}p_{66}+p_{15}+p_{16}A_{66}-\frac{B_{61}^2}{r}p_{66}p_{16} & A_{62}p_{66}+p_{16}+p_{26}A_{66}+p_{25}-\frac{B_{61}^2}{r}p_{66}p_{26} & A_{63}p_{66}+p_{26}+p_{36}A_{66}+p_{35}-\frac{B_{61}^2}{r}p_{66}p_{36} & A_{64}p_{66}+p_{36}+p_{46}A_{66}+p_{45}-\frac{B_{61}^2}{r}p_{66}p_{46} & A_{65}p_{66}+p_{46}+p_{56}A_{66}+p_{55}-\frac{B_{61}^2}{r}p_{66}p_{56} & 2(p_{66}A_{66}+p_{56})+q_6-\frac{B_{61}^2}{r}p_{66}^2 \end{bmatrix}\right\} = 0. \quad (11)$$

According to LQR control law, the closed loop state equation of the system can be represented as

$$\dot{\boldsymbol{X}}(t) = [\boldsymbol{A} - \boldsymbol{BK}]\boldsymbol{X}(t) = \left[\boldsymbol{A} - \boldsymbol{BR}^{-1}\boldsymbol{B}^T\boldsymbol{P}\right]\boldsymbol{X}(t). \quad (12)$$

The actual characteristic equation of the system can be written as:

$$|sI - \boldsymbol{A} + \boldsymbol{BK}| = 0, \quad (13)$$

$$\left|\begin{bmatrix} s & 0 & 0 & 0 & 0 & 0 \\ 0 & s & 0 & 0 & 0 & 0 \\ 0 & 0 & s & 0 & 0 & 0 \\ 0 & 0 & 0 & s & 0 & 0 \\ 0 & 0 & 0 & 0 & s & 0 \\ 0 & 0 & 0 & 0 & 0 & s \end{bmatrix} - \begin{bmatrix} 0 & 1 & 0 & 0 & 0 & 0 \\ 0 & 0 & 1 & 0 & 0 & 0 \\ 0 & 0 & 0 & 1 & 0 & 0 \\ 0 & 0 & 0 & 0 & 1 & 0 \\ 0 & 0 & 0 & 0 & 0 & 1 \\ A_{61} & A_{62} & A_{63} & A_{64} & A_{65} & A_{66} \end{bmatrix} + \begin{bmatrix} 0 & 0 & 0 & 0 & 0 & B_{61} \end{bmatrix}^T \frac{B_{61}}{r}\begin{bmatrix} p_{16} & p_{26} & p_{36} & p_{46} & p_{56} & p_{66} \end{bmatrix}\right| = 0, \quad (14)$$

$$s^6+\left(\frac{B_{61}^2}{r}p_{66}-A_{66}\right)s^5+\left(\frac{B_{61}^2}{r}p_{56}-A_{65}\right)s^4+\left(\frac{B_{61}^2}{r}p_{46}-A_{64}\right)s^3+\left(\frac{B_{61}^2}{r}p_{36}-A_{63}\right)s^2 \\ +\left(\frac{B_{61}^2}{r}p_{26}-A_{62}\right)s+\left(\frac{B_{61}^2}{r}p_{16}-A_{61}\right)=0. \tag{15}$$

Since the system considered here has two identical torsion modules, the desired characteristic equation of the sixth order system is assumed as

$$\left(s^2+2\zeta\omega_n s+\omega_n^2\right)^3=0\,, \tag{16}$$

where ζ and ω_n are the desired damping ratio and natural frequency of the system.

$$s^6+6\zeta\omega_n s^5+\left(\omega_n^2+8\omega_n^2\zeta^2+2\omega_n^2\left(1+2\zeta^2\right)\right)s^4+\left(8\zeta\omega_n^3+2\zeta\omega_n^3\left(1+2\zeta^2\right)\right)s^3 \\ +\left(\omega_n^4+8\omega_n^4\zeta^2+2\omega_n^4\left(1+2\zeta^2\right)\right)s^2+\left(\omega_n^4+8\omega_n^4\zeta^2+2\omega_n^4\left(1+2\zeta^2\right)\right)s^2+6\zeta\omega_n^5 s+\omega_n^6=0. \tag{17}$$

Comparing Equations (15) and (17), the expressions for p_{16}, $p_{26,}$ $p_{36,}$ p_{46}, p_{56}, and p_{66} can be written as:

$$p_{16}=\frac{r}{B_{61}^2}\left[A_{61}+\omega_n^6\right], \tag{18}$$

$$p_{26}=\frac{r}{B_{61}^2}\left[A_{62}+6\zeta\omega_n^5\right], \tag{19}$$

$$p_{36}=\frac{r}{B_{61}^2}\left[A_{63}+\omega_n^4+8\omega_n^4\zeta^2+2\omega_n^4\left(1+2\zeta^2\right)\right], \tag{20}$$

$$p_{46}=\frac{r}{B_{61}^2}\left[A_{64}+8\zeta\omega_n^3+2\zeta\omega_n^3\left(1+2\zeta^2\right)\right], \tag{21}$$

$$p_{56}=\frac{r}{B_{61}^2}\left[A_{65}+\omega_n^2+8\omega_n^2\zeta^2+2\omega_n^2\left(1+2\zeta^2\right)\right], \tag{22}$$

$$p_{66}=\frac{r}{B_{61}^2}\left[A_{66}+6\zeta\omega_n\right]. \tag{23}$$

From the 1st row and 1st column of ARE given in (11)

$$2\left(p_{16}A_{61}\right)+q_1-\frac{B_{61}^2}{r}p_{16}^2=0\,. \tag{24}$$

By rearranging (24), the expression for $\frac{q_1}{r}$ can be obtained as:

$$\frac{q_1}{r}=\frac{1}{B_{61}^2}\left[p_{16}^2-2\left(p_{16}A_{61}\right)\right]. \tag{25}$$

Similarly, p_{12} is obtained using the element available in 1st row 3rd column of (11).

$$p_{12} = \frac{B_{61}^2}{r} p_{36} p_{16} - p_{16} A_{63} - A_{61} p_{36} . \tag{26}$$

The element in 2nd row and 2nd column of (11) is:

$$2(p_{26} A_{62} + p_{12}) + q_2 - \frac{B_{61}^2}{r} p_{26}^2 = 0 . \tag{27}$$

Substituting (26) into (27) and rearranging the expression yields

$$\frac{q_2}{r} = \frac{1}{B_{61}^2} \left[p_{26}^2 - 2\left(p_{26} A_{62} + p_{36} p_{16} - p_{16} A_{63} - A_{61} p_{36} \right) \right]. \tag{28}$$

Likewise, the element available in 3rd row and 3rd column of (11) can be written as:

$$2(p_{36} A_{63} + p_{23}) + q_3 - \frac{B_{61}^2}{r} p_{36}^2 = 0 . \tag{29}$$

Expressions for p_{23} and p_{14} are obtained from 2nd row and 4th column and 1st row and 5th column of (11) respectively.

$$p_{23} = \frac{B_{61}^2}{r} p_{46} p_{26} - A_{62} p_{46} - p_{14} - p_{26} A_{64} , \tag{30}$$

$$p_{14} = \frac{B_{61}^2}{r} p_{56} p_{16} - A_{61} p_{56} - p_{16} A_{65} . \tag{31}$$

Substituting (30) and (31) into Equation (29) and rearranging

$$\frac{q_3}{r} = \frac{1}{B_{61}^2} \left[p_{36}^2 - 2\left(p_{36} A_{63} + p_{46} p_{26} - A_{62} p_{46} - p_{56} p_{16} + A_{61} p_{56} + p_{16} A_{65} - p_{26} A_{64} \right) \right]. \tag{32}$$

Similarly, the element available in 4th row and 4th column of (11) can be written as:

$$2(p_{46} A_{64} + p_{34}) + q_4 - \frac{B_{61}^2}{r} p_{46}^2 = 0 . \tag{33}$$

The terms p_{34}, p_{25} are obtained from 3rd row 5th column and 2nd row 6th column respectively from (11).

$$p_{34} = \frac{B_{61}^2}{r} p_{56} p_{36} - A_{63} p_{56} - p_{25} - p_{36} A_{65} , \tag{34}$$

$$p_{25} = \frac{B_{61}^2}{r} p_{66} p_{26} - A_{62} p_{66} - p_{16} - p_{26} A_{66} . \tag{35}$$

Substituting (34) and (35) into equation (33) and rearranging,

$$\frac{q_4}{r}=\frac{1}{B_{61}^2}\left[p_{46}^2-2\left(p_{46}A_{64}+p_{56}p_{36}-A_{63}p_{56}-p_{66}p_{26}+A_{62}p_{66}+p_{16}+p_{26}A_{66}-p_{36}A_{65}\right)\right]. \quad (36)$$

The element available in 5th row and 5th column of (11) is

$$2(p_{56}A_{65}+p_{45})+q_5-\frac{B_{61}^2}{r}p_{56}^2=0. \quad (37)$$

The term p_{45} is obtained from 4th row 6th column from (11).

$$p_{45}=\frac{B_{61}^2}{r}p_{66}p_{46}-A_{64}p_{66}-p_{36}-p_{46}A_{66}. \quad (38)$$

Substituting (38) into (37) and rearranging,

$$\frac{q_5}{r}=\frac{1}{B_{61}^2}\left[p_{56}^2-2\left(p_{56}A_{65}+p_{66}p_{46}-A_{64}p_{66}-p_{36}-p_{46}A_{66}\right)\right]. \quad (39)$$

Similarly, from the element available in 6th row and 6th column of (11),

$$2(p_{66}A_{66}+p_{56})+q_6-\frac{B_{61}^2}{r}p_{66}^2=0. \quad (40)$$

Upon rearranging,

$$\frac{q_6}{r}=\frac{1}{B_{61}^2}\left[p_{66}^2-2\left(p_{66}A_{66}+p_{56}\right)\right]. \quad (41)$$

The expressions (25), (28), (32), (36), (39) and (41) exhibit the relation between $\boldsymbol{Q}$ and $\boldsymbol{R}$ weighting matrices of LQR and the design requirements in time domain and state model. Equation (42) summarizes the expressions for weighting matrices.

$$\begin{aligned}
&\frac{q_1}{r}=\frac{1}{B_{61}^2}\left[p_{16}^2-2\left(p_{16}A_{61}\right)\right],\\
&\frac{q_2}{r}=\frac{1}{B_{61}^2}\left[p_{26}^2-2\left(p_{26}A_{62}+p_{36}p_{16}-p_{16}A_{63}-A_{61}p_{36}\right)\right],\\
&\frac{q_3}{r}=\frac{1}{B_{61}^2}\left[p_{36}^2-2\left(p_{36}A_{63}+p_{46}p_{26}-A_{62}p_{46}-p_{56}p_{16}+A_{61}p_{56}+p_{16}A_{65}-p_{26}A_{64}\right)\right],\\
&\frac{q_4}{r}=\frac{1}{B_{61}^2}\left[p_{46}^2-2\left(p_{46}A_{64}+p_{56}p_{36}-A_{63}p_{56}-p_{66}p_{26}+A_{62}p_{66}+p_{16}+p_{26}A_{66}-p_{36}A_{65}\right)\right],\\
&\frac{q_5}{r}=\frac{1}{B_{61}^2}\left[p_{56}^2-2\left(p_{56}A_{65}+p_{66}p_{46}-A_{64}p_{66}-p_{36}-p_{46}A_{66}\right)\right],\\
&\frac{q_6}{r}=\frac{1}{B_{61}^2}\left[p_{66}^2-2\left(p_{66}A_{66}+p_{56}\right)\right].
\end{aligned} \quad (42)$$

The elements of $\boldsymbol{Q}$ matrix can be obtained using the desired specifications by fixing the

value of ***R*** matrix which is taken as scalar in the present example because the plant taken for experimentation is a single input multi output system. It can be observed that the expression (42) yields a simple relation to select the elements of penalty matrices according to the design criteria given in time domain. Hence, from the design perspective, knowing the desired damping ratio, natural frequency of the system and the state space matrices of the plant, one can determine the elements of weighting matrices and in turn the optimal controller gain (***K***) can be obtained using (6) by solving the ARE. In the next section, the validation of the proposed algebraic weight selection algorithm on a 2 DoF torsion system for tracking application is presented.

4. LQR tracking control of 2 DoF torsion system

The 2 DoF torsion system, as shown in Fig. 1, consists of a DC motor whose shaft is attached to a series of torsion modules via flexible linkage. Table 1 gives the nominal plant parameters of the 2 DoF torsion system. When the voltage given to the motor is varied, the corresponding shaft position varies, which in turn alters the position of the torsion modules.

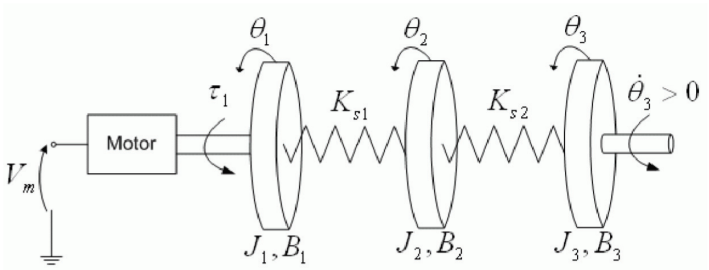

Fig. 1. Schematic diagram of 2-DoF torsion system

Applying Newton's second law to the schematic diagram shown in Fig. 1, and assuming the states $\boldsymbol{X} = \begin{bmatrix}\theta_1 & \theta_2 & \theta_3 & \dot{\theta}_1 & \dot{\theta}_2 & \dot{\theta}_3\end{bmatrix}^T$ and the input $U = V_m$, we obtain the following state space model:

$$\begin{bmatrix}\dot{\theta}_1\\ \dot{\theta}_2\\ \dot{\theta}_3\\ \ddot{\theta}_1\\ \ddot{\theta}_2\\ \ddot{\theta}_3\end{bmatrix} = \begin{bmatrix} 0 & 0 & 0 & 1 & 0 & 0\\ 0 & 0 & 0 & 0 & 1 & 0\\ 0 & 0 & 0 & 0 & 0 & 1\\ \dfrac{-K_{s1}}{J_1} & \dfrac{K_{s1}}{J_1} & 0 & \dfrac{-B_1}{J_1} & 0 & 0\\ \dfrac{K_{s1}}{J_2} & \dfrac{-(K_{s1}+K_{s2})}{J_2} & \dfrac{K_{s2}}{J_2} & 0 & \dfrac{-B_2}{J_2} & 0\\ 0 & \dfrac{K_{s2}}{J_3} & \dfrac{-K_{s2}}{J_3} & 0 & 0 & \dfrac{-B_3}{J_3}\end{bmatrix}\begin{bmatrix}\theta_1\\ \theta_2\\ \theta_3\\ \dot{\theta}_1\\ \dot{\theta}_2\\ \dot{\theta}_3\end{bmatrix} + \begin{bmatrix}0\\ 0\\ 0\\ \dfrac{1}{J_1}\\ 0\\ 0\end{bmatrix} V_m, \qquad (43)$$

$$\boldsymbol{Y} = \begin{bmatrix} 1 & 0 & 0 & 0 & 0 & 0 \\ 0 & 1 & 0 & 0 & 0 & 0 \\ 0 & 0 & 1 & 0 & 0 & 0 \end{bmatrix} \begin{bmatrix} \theta_1 \\ \theta_2 \\ \theta_3 \\ \dot{\theta}_1 \\ \dot{\theta}_2 \\ \dot{\theta}_3 \end{bmatrix}. \tag{44}$$

Table 1. List of parameters of 2-DoF torsion system

Symbol	Description	Value	Unit
J_1	Equivalent moment of inertia as seen at SRV02 load shaft	0.0022	Kg · m^2
B_1	Equivalent viscous damping coefficient as seen at SRV02 load shaft	0.0150	N.m.s/rad
J_2	Equivalent moment of inertia from the torsion module-1	$5.46 \cdot 10^{-4}$	Kg · m^2
B_2	Equivalent viscous damping coefficient as seen at SRV02 load shaft	0.0010	N · m · s/rad
J_3	Equivalent moment of inertia from torsion module-2	$5.45 \cdot 10^{-4}$	Kg · m^2
B_3	Equivalent viscous damping coefficient as seen at SRV02 load shaft	0.0030	N · m · s/rad
K_{s1}	First flexible coupling stiffness	1.0000	N · m/rad
K_{s2}	Second flexible coupling stiffness	1.0000	N · m/rad

Figure 2 depicts the proposed LQR controller framework for tracking control of torsion system. The system consists of an LQR controller whose weights are determined using the algebraic approach and an HGO which estimates the unmeasured angular velocities. The following section explains the need and design of HGO in torsion system.

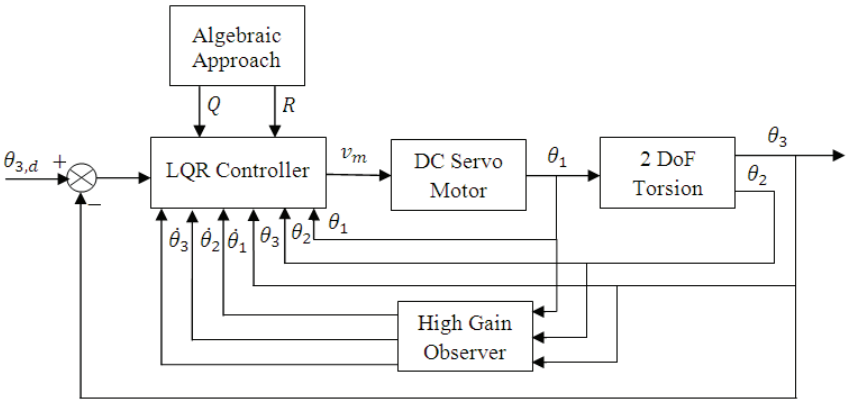

Fig. 2. Proposed controller strategy for tracking control of 2 DoF torsion

4.1. High gain observer

To implement LQR control, full state vector information must be available for feedback. The 2 DoF torsion system has six state variables, namely three angular positions and three angular velocities. The torsion angular positions can be measured accurately using the position encoders. However, the angular velocities are normally determined either by differentiating the measured angular position or through tachometers in practical cases. In both the cases, the velocity signal is contaminated by noise, and this degrades the performance of the closed loop torsion system [21]. Hence, an HGO is included in the feedback path to estimate the angular velocities of torsional loads.

The state variables of the system can be grouped as position and velocity vectors, namely $\boldsymbol{X}_p$ and $\boldsymbol{X}_v$.

$$\boldsymbol{X}_p = \theta = \begin{bmatrix} \theta_1 \\ \theta_2 \\ \theta_3 \end{bmatrix}, \tag{45}$$

$$\boldsymbol{X}_v = \dot{\theta} = \begin{bmatrix} \dot{\theta}_1 \\ \dot{\theta}_2 \\ \dot{\theta}_3 \end{bmatrix}. \tag{46}$$

The output vector is:

$$\boldsymbol{Y} = \boldsymbol{X}_p = \begin{bmatrix} \theta_1 \\ \theta_2 \\ \theta_3 \end{bmatrix}. \tag{47}$$

The equation of motion of torsion system can be expressed in state space form as:

$$\boldsymbol{X}_v = \dot{\boldsymbol{X}}_p, \tag{48}$$

$$\dot{\boldsymbol{X}}_v = \Phi(\boldsymbol{X}_p, \boldsymbol{X}_v, \boldsymbol{u}), \tag{49}$$

$$\boldsymbol{Y} = \boldsymbol{X}_p. \tag{50}$$

The structure of the HGO is:

$$\dot{\hat{\boldsymbol{X}}}_p = \hat{\boldsymbol{X}}_v + \boldsymbol{H}_p\left(\boldsymbol{Y} - \hat{\boldsymbol{X}}_p\right), \tag{51}$$

$$\dot{\hat{\boldsymbol{X}}}_v = \boldsymbol{H}_v\left(\boldsymbol{Y} - \hat{\boldsymbol{X}}_p\right) + \Phi(\boldsymbol{X}_p, \boldsymbol{X}_v, t), \tag{52}$$

where $\dot{\hat{\boldsymbol{X}}}_p$ and $\dot{\hat{\boldsymbol{X}}}_v$

represent the dynamic estimates of the angular positions and angular velocities, respectively. The HGO consists of two constant gain matrices, $\boldsymbol{H}_p$ and $\boldsymbol{H}_v$. which are assumed to be a diagonal matrix as given below.

$$\boldsymbol{H}_p = \begin{bmatrix} h_{p1} & 0 & 0 \\ 0 & h_{p2} & 0 \\ 0 & 0 & h_{p3} \end{bmatrix}; \quad H_v = \begin{bmatrix} h_{v1} & 0 & 0 \\ 0 & h_{v2} & 0 \\ 0 & 0 & h_{v3} \end{bmatrix}. \tag{53}$$

The convergence rate of the HGO can be varied by adjusting the gain matrices $\boldsymbol{H}_p$ and $\boldsymbol{H}_v$. The error between the actual states and estimated states via HGO is given as:

$$\dot{\tilde{\boldsymbol{X}}}_p = -\boldsymbol{H}_p \tilde{\boldsymbol{X}}_p + \tilde{\boldsymbol{X}}_v, \tag{54}$$

$$\dot{\tilde{\boldsymbol{X}}}_v = -\boldsymbol{H}_v \tilde{\boldsymbol{X}}_p + \delta(\boldsymbol{X}, \hat{\boldsymbol{X}}), \tag{55}$$

where:

$$\delta(\boldsymbol{X}, \hat{\boldsymbol{X}}) = \Phi(\boldsymbol{X}_p, \boldsymbol{X}_v, \boldsymbol{u}) - \Phi_0(\hat{\boldsymbol{X}}_p, \hat{\boldsymbol{X}}_v, \boldsymbol{u}) \text{ and } \tilde{\boldsymbol{X}}_i = \boldsymbol{X}_i - \hat{\boldsymbol{X}}_i,\ i = 1, 2, 3.$$

In the absence of disturbance signal, the asymptotic error convergence can be achieved by selecting the observer gain matrix given in (56) as Hurwitz [22]. Moreover, to guarantee the convergence of the error dynamic equation, the eigenvalues of matrix $\boldsymbol{F}$ should be located on the left half of s-plane.

$$\boldsymbol{F} = \begin{bmatrix} -\boldsymbol{H}_p & I_{3\times3} \\ -\boldsymbol{H}_v & 0_{3\times3} \end{bmatrix}. \tag{56}$$

5. Experimental results and discussion

The test bed consists of a Quanser SRV02 rotary servo base unit, Q8 data acquisition board, power amplifier and two torsion modules. Fig. 3 illustrates the connection diagram of experimental setup. The rotary servo base unit contains a 10 V DC motor equipped with the internal gearbox. The torsional load consists of two inertial disc masses which are located at different anchor points along the support bar. To measure the angular positions, both the DC motor and the torsion modules have optical encoders, which offer a resolution of 4096 counts per revolution. The Q8 USB hardware-in-loop (HIL) data acquisition board has 8 digital inputs and 8 pulse width modulated (PWM) digital outputs, and it is capable of reaching 4 kHz sampling rate. The control algorithm implemented in SIMULINK communicates with the hardware using QUARC interfacing software. In addition, the system contains a Volt-PAQ power amplifier, which provides a regulated ±10 V at 1 A, to amplify the control signal given to the DC motor.

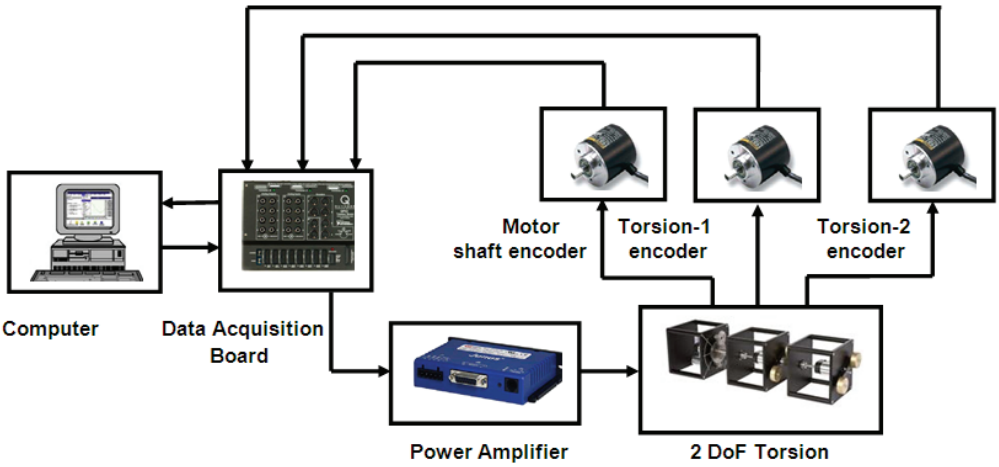

Fig. 3. Connection Diagram of 2-DoF torsion system

By substituting the plant parameters given in Table 1 into the state space model given in (45) and (46), the following state space matrices are obtained.

$$\boldsymbol{A}=\begin{bmatrix} 0 & 0 & 0 & 1 & 0 & 0 \\ 0 & 0 & 0 & 0 & 1 & 0 \\ 0 & 0 & 0 & 0 & 0 & 1 \\ -457.8 & 457.8 & 0 & -6.9 & 0 & 0 \\ 1831.1 & -3662.2 & 1831.1 & 0 & -1.8 & 0 \\ 0 & 1883.6 & -1883.6 & 0 & 0 & -5.5 \end{bmatrix}, \quad \boldsymbol{B}=\begin{bmatrix} 0 \\ 0 \\ 0 \\ 457.84 \\ 0 \\ 0 \end{bmatrix},$$

$$\boldsymbol{C}=\begin{bmatrix} 1 & 0 & 0 & 0 & 0 & 0 \\ 0 & 1 & 0 & 0 & 0 & 0 \\ 0 & 0 & 1 & 0 & 0 & 0 \end{bmatrix}.$$

Then, the above model is transformed into following controllable canonical form:

$$\boldsymbol{A}=\begin{bmatrix} 0 & 1 & 0 & 0 & 0 & 0 \\ 0 & 0 & 1 & 0 & 0 & 0 \\ 0 & 0 & 0 & 1 & 0 & 0 \\ 0 & 0 & 0 & 0 & 1 & 0 \\ 0 & 0 & 0 & 0 & 0 & 1 \\ -1.4\times10^{-7} & -2.9\times10^{7} & -5.2\times10^{6} & -6.4\times10^{4} & 6014 & -14.2 \end{bmatrix}, \quad \boldsymbol{B}=\begin{bmatrix} 0 \\ 0 \\ 0 \\ 0 \\ 0 \\ 1.5\times10^{9} \end{bmatrix},$$

$$\boldsymbol{C} = \begin{bmatrix} 1 & 0 & 0 & 0 & 0 & 0 \\ 0 & 1 & 0 & 0 & 0 & 0 \\ 0 & 0 & 1 & 0 & 0 & 0 \end{bmatrix}.$$

The design requirement of the control scheme is that it should provide a tracking response, which has an overshoot of less than 10% and a settling time of 0.6 sec. Moreover, the tracking error should be less than 5 deg (2% criterion of the torsion load angle), and the control effort should not reach the saturation level when the above criteria are met. To compute the state feedback gain for the above design requirement, first, the damping ratio of the system is determined using the 2% criterion of settling time, and it is calculated as 0.1. Then, using the corresponding damping ratio and natural frequency, the desired characteristic equation is formulated, and with the aid of the proposed algebraic approach the following $\boldsymbol{Q}$ and $\boldsymbol{R}$ weighing matrices are obtained.

$$\boldsymbol{Q} = \begin{bmatrix} 5.04 & 0 & 0 & 0 & 0 & 0 \\ 0 & 6.08 & 0 & 0 & 0 & 0 \\ 0 & 0 & 2.49 & 0 & 0 & 0 \\ 0 & 0 & 0 & 0.33 & 0 & 0 \\ 0 & 0 & 0 & 0 & 6\times10^{-6} & 0 \\ 0 & 0 & 0 & 0 & 0 & 4\times10^{-10} \end{bmatrix}, \quad \boldsymbol{R} = [200],$$

Using the above weighing matrices and the state space model of the system, the solution of ARE ($\boldsymbol{P}$) and the state feedback gain matrix ($\boldsymbol{K}$) are calculated and given below.

$$\boldsymbol{P} = 10^5 \times \begin{bmatrix} 2441.4 & 0 & 0 & 0 & 0 & 0 \\ 0 & 4.3 & 0 & 0 & 0 & 0 \\ 0 & 0 & 2959.7 & 0 & 0 & 0 \\ 0 & 0 & 0 & 65.4 & 0 & 0 \\ 0 & 0 & 0 & 0 & 4.7 & 0 \\ 0 & 0 & 0 & 0 & 0 & 0.01 \end{bmatrix},$$

$$\boldsymbol{K} = [0.15 \quad 0.29 \quad 0.19 \quad 0.04 \quad 0.0003 \quad 7.7\times10^{-6}].$$

Gain matrices of the HGO to estimate the velocity component of the system are found to be:

$$\boldsymbol{H}_p = \begin{bmatrix} 10 & 0 & 0 \\ 0 & 16 & 0 \\ 0 & 0 & 23 \end{bmatrix}, \quad \boldsymbol{H}_v = \begin{bmatrix} 12 & 0 & 0 \\ 0 & 27 & 0 \\ 0 & 0 & 34 \end{bmatrix}.$$

The corresponding eigenvalues of the closed loop system are:

$$\lambda_{cl} = \begin{bmatrix} -398.76 & -398.26+0.29i & -398.26-0.29i & -1.6+0.05i & -1.6-0.05i & -1.5 \end{bmatrix}.$$

It is worth to note that the first three eigenvalues are placed far away from the imaginary axis of s-plane. Hence, it will assist in improving the speed of response of the system. Similarly, three eigenvalues which are placed sufficiently close to imaginary axis will aid in reducing the amount of control input given to the system. Before implementing the proposed control framework in real time, the simulation was carried out in MATLAB. On verifying that the design meets the specification, we also have implemented it on a real time 2 DoF torsion system.

5.1. Trajectory tracking

To test the tracking response of the controller, a square trajectory with amplitude of 300 deg at a frequency of 0.1 Hz is given as a reference signal. Fig. 4 shows both the simulated and experimental tracking response of the controller for the square wave trajectory. Simulated angular position response has an overshoot of 4.16% with a settling time of 0.88 sec, whereas the overshoot of the experimental output is 9.6% with a settling time is 0.92 sec. It is worth to note that the experimental results meet the design requirements both interms of steady state error and overshoot. However, there is a small deviation in real time output from the simulated one due to the presence of noise in measurement. To assess the reference following performance of the control scheme, the integral square error (ISE) is calculated and given in Table 2. Fig. 5 illustrates the estimated velocities of the torsion system using HGO and Table 3 gives the tracking error of HGO for all three velocities. Minimum value of IAE suggests that the estimated output is very close to the actual output.

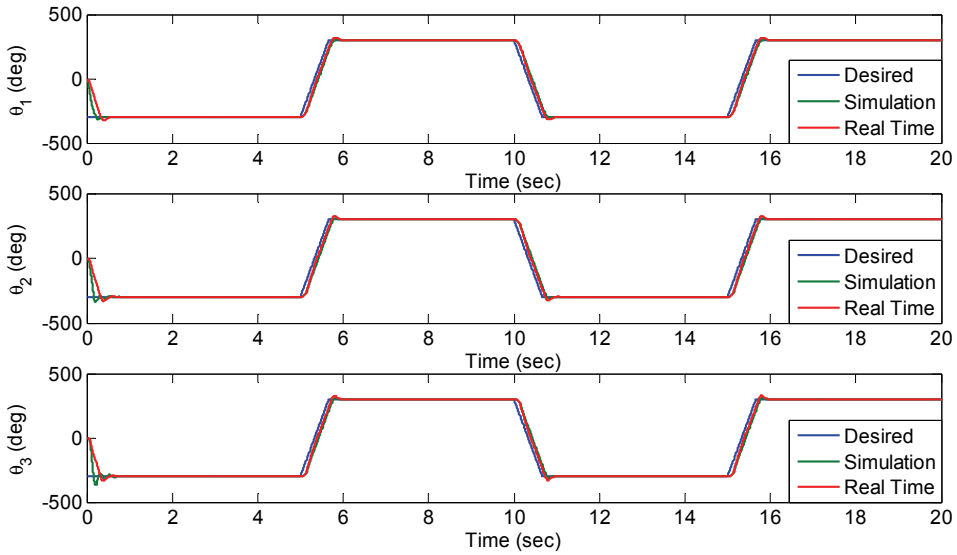

Fig. 4. Square trajectory tracking response

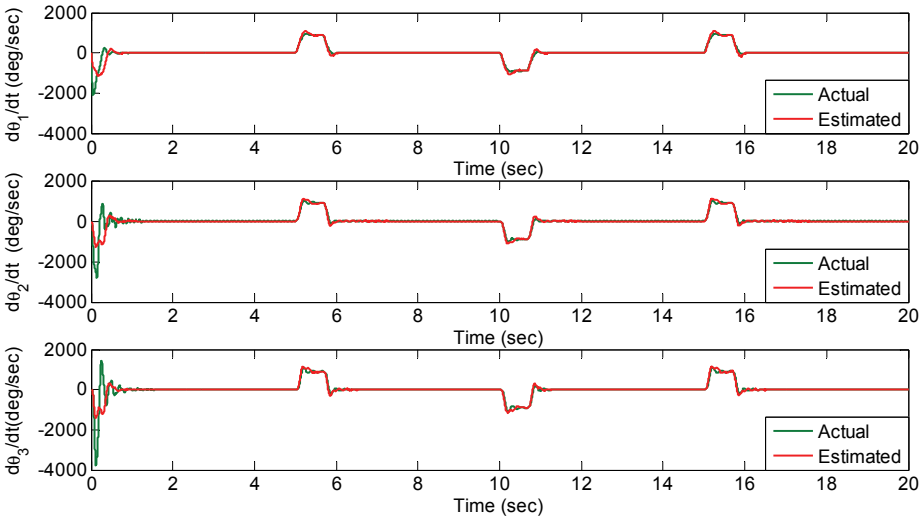

Fig. 5. Estimated velocities of HGO for square trajectory

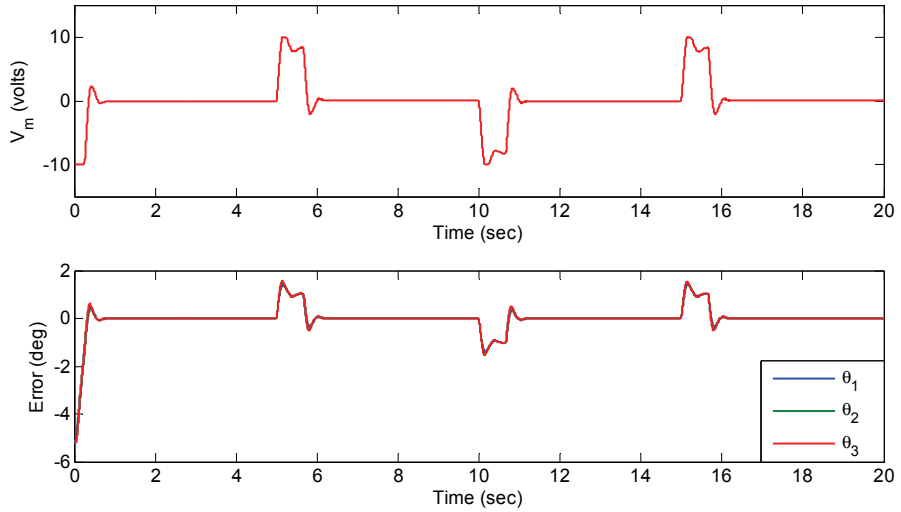

Fig. 6. Control signal and tracking error of square trajectory

The control input applied to motor for tracking the desired tracjectory and the error between the reference trajectory and actual trajectory signal are shown in Fig. 6. The maximun tracking error is found to be less than 1.5 deg, which accentuates that the controller effectively follows the given trajectory.

5.2. Sinusoidal trajectory

The performance of the controller framework to track the continuously changing reference signal is validated using a sinusoidal signal of amplitude 300 deg at a frequency of 0.1 Hz.

Fig. 7, which shows the sinusoidal tracking response, highlights that the LQR controller closely tracks the reference trajectory. The estimated velocities of HGO and the control signal applied to DC servo along with the tracking error are shown in Figs. 8 and 9, respectively. It can be seen that the rate of convergence of the system is faster with the maximum tracking error of 0.3 deg, which is negligible in case of torsional position control applications. Moreover, the error converges exactly to desired trajectory variations with very minimal spikes occuring concurrently at random intervals due to the presence of noise in real time.

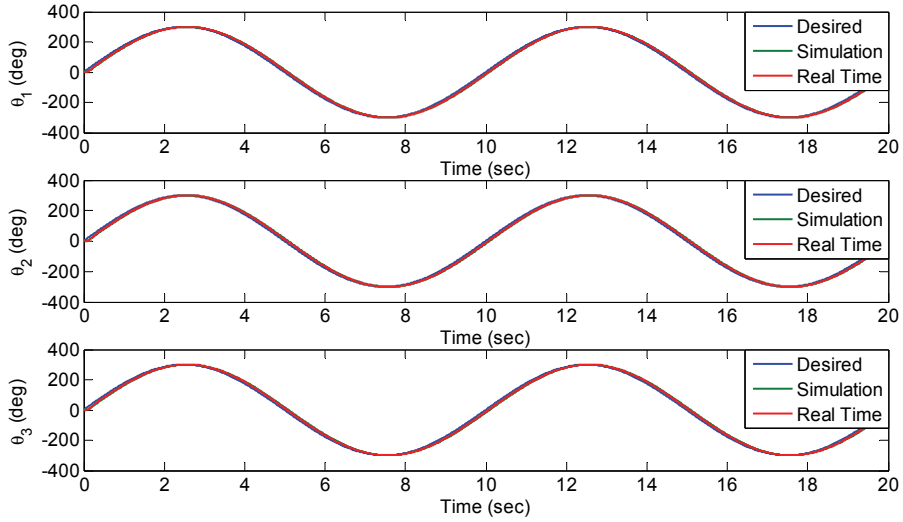

Fig. 7. Sinusoidal tracking response

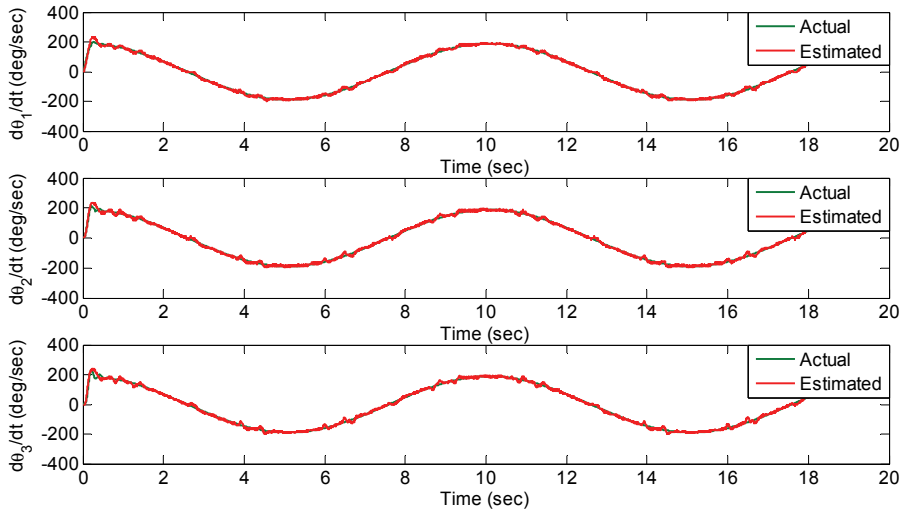

Fig. 8. HGO response for sinusoidal trajectory

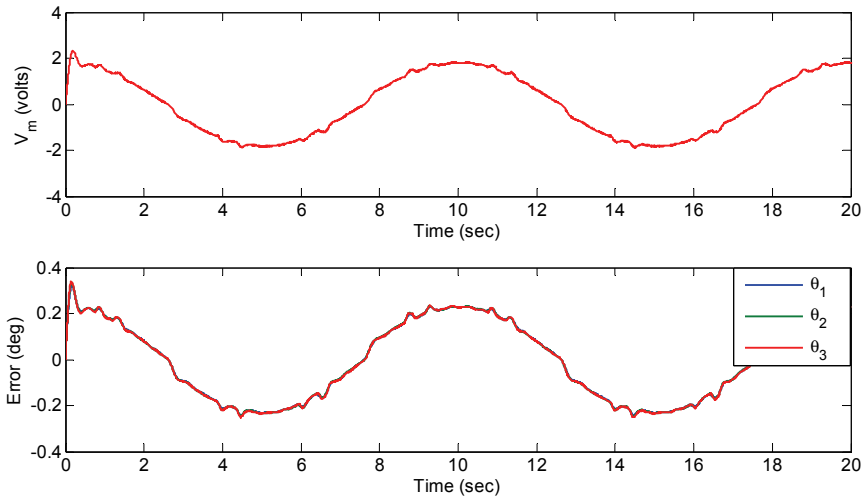

Fig. 9. Control signal and tracking error of sine trajectory

Table 2. ISE of LQR control scheme for test trajectories

Test signal	**Simulation**	**Real Time**
Square	0.0007	0.0029
Sine	0.0015	0.0022

Table 3. IAE of HGO for test trajectories

Test signal	θ_1	θ_2	θ_3
Square	0.0312	0.0215	0.0351
Sine	0.0231	0.0226	0.0218

6. Conclusion

Even though the optimal performance of LQR is highly dependent on weighting matrices Q and R, normally, these weighting matrices are chosen based on the trial and error approach, which is not only tedious but also time consuming. Hence, in this paper, to address the weight selection problem of LQR, we have put forward an algebraic weight selection algorithm, by synthesizing the ARE with the Lagrange optimization technique. Simple mathematical expressions for weighting matrices have been obtained as a function of the design criteria and state model. The efficacy of the proposed methodology has been tested on a benchmark 2 DoF torsion system for tracking applications. To estimate the angular velocities of servo and torsional loads, an HGO has been integrated with the LQR design. Two test cases namely sine and square trajectories have been given as a reference signal and the efficacy of the control scheme to follow the input with minimal vibration and error has been assessed. The experi-

mental results accentuate that the proposed control scheme can make the torsional load meet the design criteria with minimal vibrations and reduced tracking error.

References

[1] da Fonseca Neto J.V., Abreu I.S., da Silva F.N., *Neural-Genetic Synthesis for State-Space Controllers Based on Linear Quadratic Regulator Design for Eigenstructure Assignment*, IEEE Transactions on Systems, Man, and Cybernetics–Part B: Cybernetics, vol. 40, no. 2, pp. 266-285 (2010).

[2] Das S., Pan I., Halder K., Das S., Gupta A., *LQR based improved discrete PID controller design via optimum selection of weighting matrices using fractional order integral performance index*, Applied Mathematical Modelling, vol. 37, no. 6, pp. 4253-4268 (2013).

[3] Bevilacqua R., Lehmann T., Romano M., *Development and experimentation of LQR/APF guidance and control for autonomous proximity maneuvers of multiple spacecraft*, Acta Astronautica, vol. 68, no. 8, pp. 1260-1275 (2011).

[4] Tao C., Taur J., Chen Y., *Design of a parallel distributed fuzzy LQR controller for the twin rotor multi-input multi-output system,* Fuzzy Sets and Systems, vol. 161, no. 15, pp. 2081-2103 (2010).

[5] Balandat M., Zhang W., Abate A., *On infinite horizon switched LQR problems with state and control constraints,* Systems & Control Letters, vol. 61, no. 4, pp. 464-471 (2012).

[6] Wang L., Ni H., Zhou W., Pardalos P.M., Fang J., Fei M., *MBPOA-based LQR controller and its application to the double-parallel inverted pendulum system,* Engineering Applications of Artificial Intelligence, vol. 36, pp. 262-268 (2014).

[7] Niknezhadi A., Allué-Fantova M., Kunusch C., Ocampo-Martínez C., *Design and implementation of LQR/LQG strategies for oxygen stoichiometry control in PEM fuel cells based systems*, Journal of Power Sources, vol. 196, no. 9, pp. 4277-4282 (2011).

[8] Liu H., Lu G., Zhong Y., *Robust LQR Attitude Control of a 3-DoF Laboratory Helicopter for Aggressive Maneuvers*, IEEE Transactions on Industrial Electronics, vol. 60, no. 10, pp. 4627-4636 (2013).

[9] Sunar M., Rao S.S., *Optimal Selection of Weighting Matrices in Integrated Design of Structures/ Controls*, AIAA Journal, vol. 31, no. 4, pp. 714-720 (1993).

[10] Ohta H., Kakinuma M., Nikiforuk P.N., *Use of Negative Weights in Linear Quadratic Regulator Synthesis*, Journal of Guidance, Control and Dynamics, vol. 14, no. 4, pp. 791-796 (1991).

[11] Ochi Y., Kanai K., *A New Way of Pole Placement in LQR and its Application to Flight Control*, Proc. Conf. AIAA Guidance, Navigation and Control, pp. 1295-1301 (1993).

[12] Hiroe T., Morimoto T., Inoue S.I., Takamatsu H., *A New Method for Selecting Weighting Matrices of LQ Regulators and its Application to an Industrial Turbine*, Proc. 32nd Conf. on Decision and Control, pp. 3333-3334 (1993).

[13] Choi J.W., Seo Y.B., *LQR Design with Eigenstructure Assignment Capability*, IEEE Transactions on Aerospace and Electronic System, vol. 35, no. 2, pp. 700-708 (1999).

[14] Ang K.K., Wang S.Y., Quek S.T., *Weighted Energy Linear Quadratic Regulator Vibration Control of Piezoelectric Composite Plates*, Smart Materials and Structures, vol. 11, no. 1, pp. 98-106 (2002).

[15] Robandia I., Nishimori K., Nishimura R., Ishihara N., *Optimal feedback control design using genetic algorithm in multimachine power system*, Electrical Power and Energy Systems, vol. 23, no. 4, pp. 263-271 (2001).

[16] Panda S., Padhy N.P., *Comparison of particle swarm optimization and genetic algorithm for FACTS-based controller design*, Applied Soft Computing, vol. 8, no. 4, pp. 1418-1427 (2008).

[17] Tsai S.J., Huo C.L., Yang Y.K., Sun T.Y., *Variable feedback gain control design based on particle swarm optimizer for automatic fighter tracking problems*, Applied Soft Computing, vol. 13, no. 1, pp. 58-75 (2013).

[18] Vinodh K.E., Jerome J., *An Adaptive Particle Swarm Optimization Algorithm for Robust Trajectory Tracking of a Class of Under Actuated System*, Archives of Electrical Engineering, vol. 63, no. 3, pp. 345-365 (2014).

[19] Desineni S.N., *Optimal Control Systems*, CRC press (2003).
[20] Oral O., Çetin L., Uyar E., *A novel method on selection of Q And R matrices in the theory of optimal control*, International Journal of Systems Control, vol. 1, no. 2, pp. 84-92 (2010).
[21] Wang G., *Observer based feedback control methods for an under actuated robot system. M.S Thesis*, Simon Fraser University, Canada, November (2003).
[22] Khalil H.K., Praly L., *High gain observers in nonlinear feedback control*, International Journal of Robust and Nonlinear Control, vol. 24, no. 6, pp. 993-1015 (2014).